SCIENTIFIC REPORTS

OPEN

Structural and electronic properties of $Mo_6S_3I_6$ nanowires by newly proposed theoretical compositional ordering

Received: 23 September 2018
Accepted: 13 December 2018
Published online: 04 February 2019

You Kyoung Chung[1], Weon-Gyu Lee[1], Sudong Chae[2], Jae-Young Choi[2,3] & Joonsuk Huh[1]

The structural, electronic, and magnetic properties of molybdenum-based nanowires have been actively investigated for their potential applications in nanodevices; however, further advancement is hindered by incomplete knowledge of the electronic and atomic structures of $Mo_6S_3I_6$. To facilitate further development of $Mo_6S_3I_6$ nanowire devices, we propose possible atomic structures and corresponding electronic properties of $Mo_6S_3I_6$ nanowires based on density functional theory. We explored various combinations of atomic structures by changing the positions of sulfur and iodine atoms linked to the two Mo_6 octahedra in the $Mo_6S_3I_6$ unit cell. We found two stable local energy minima structures characterized by elongation of the wire length, and therefore propose 28 possible atomic configurations. We calculated band structures of the newly proposed atomic models and found three structures that behaved as conductors. According to our compositional ordering structural analysis, we concluded that (i) periodic distortion of the bond lengths influences the behavior of the electrons in the system, (ii) the role of sulfur atoms in the bridging plane is important for intramolecular charge transport due to delocalized charge differences, and (iii) the electronic band gap energy is proportional to the integrated Mo-S bonding orbital energy.

The structural and electronic properties of one-dimensional materials such as $LiMo_3Se_3$, $Mo_6S_{9-x}I_x$ have been widely investigated since molybdenum-based transition metal dichalcogenides (TMDCs) nanowires emerged in molecular electronics[1–8]. Unlike $LiMo_3Se_3$, which is composed of ionic bonds and decomposes rapidly in air, $Mo_6S_{9-x}I_x$ can be prepared as a non-defective, uniform substance due to its air stability[9] and the van der Waals interactions between its chains. Although the extraordinary stability of $Mo_6S_{9-x}I_x$ is well known, the details of its structure that lead to this stability remain unknown.

In an early study of $Mo_6S_{9-x}I_x$ nanowires, Milhailovic *et al.* revealed that $Mo_6S_3I_6$ behaves as a quasi-one-dimensional conductor in the entire range of the study's targeted strains[9,10], and isomers of $Mo_{12}S_9I_9$ were identified either as conductors or narrow-gap semiconductors[11]. Tománek *et al.* found $Mo_6S_3I_6$ with sulfur atoms positioned in Mo-S-Mo bridges are particularly stable and identified $Mo_6S_{4.5}I_{4.5}$ as a conductor[12]. An additional study regarding the effect of the inter-wire interaction showed that some particular isomers of bundled $Mo_6S_{4.5}I_{4.5}$ and an isolated $Mo_6S_3I_6$ nanowire are conductors[13]. In a later study by Muragan *et al.*[14], the role of the valence electron concentration (VEC) on the structural stability and electronic properties of $Mo_6S_{9-x}I_x$ nanowires was discussed, and $Mo_6S_{7.5}I_{1.5}$ was reported as a conductor. However, the crystallographic structure of $Mo_6S_3I_6$ nanowires is still uncertain because the positions of sulfur and iodine atoms have not been precisely determined by any experimental structural analysis methods such as field emission microscopy[15] or x-ray diffraction[16].

To provide a better understanding on the atomic structure of $Mo_6S_3I_6$, we performed density function theory (DFT) calculations and obtained two stable structures at local energy minima dependent on the elongation of Mo-S-Mo bond, which is different from the result of Tománek *et al.*[17] Based on these two stable structures, we propose various new structural models of $Mo_6S_3I_6$ nanowires, by changing the decorative and bridging sites of sulfur and iodine atoms linked to the two Mo_6 octahedra in the unit cell as shown in Fig. 1. In this work, we

[1]Department of Chemistry, Sungkyunkwan University, Suwon, 16419, Korea. [2]School of Advanced Materials Science & Engineering, Sungkyunkwan University, Suwon, 16419, Republic of Korea. [3]SKKU Advanced Institute of Nanotechnology (SAINT), Sungkyunkwan University, Suwon, 16419, Republic of Korea. Correspondence and requests for materials should be addressed to J.-Y.C. (email: jy.choi@skku.edu) or J.H. (email: joonsukhuh@skku.edu)

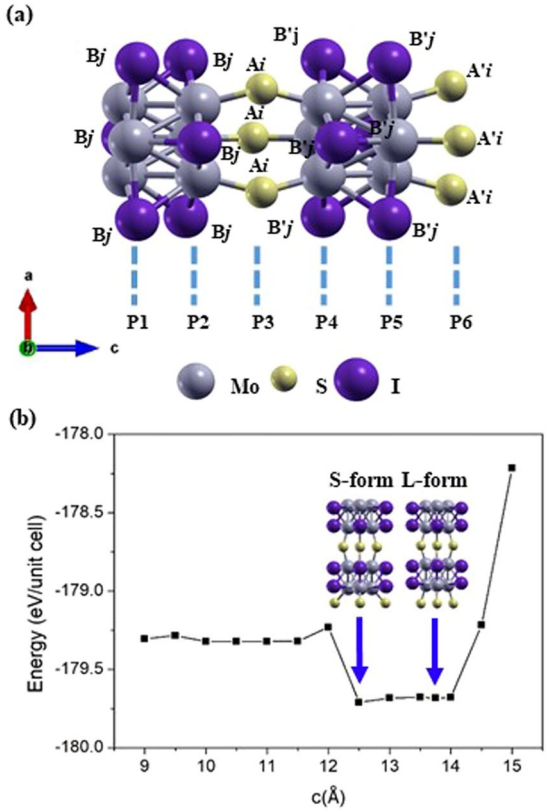

Figure 1. (**a**) Schematic atomic arrangement of the $Mo_6S_3I_6$ nanowire unit cell used as a starting point for structural calculations. The unit cell contains 2 formula units, which includes 30 atoms arranged to form two Mo_6 octahedra. The decorative and bridging sites of sulfur and iodine atoms linked to the two Mo_6 octahedra in the unit cell are labeled as B*j*, B′*j* and A*i*, A′*i*, where $i = 0–3$ and $j = 1–6$. (**b**) Total energy per unit cell of $Mo_6S_3I_6$ as a function of the lattice constant c, showing two local minima at c = 12.50 Å, and c = 13.75 Å. The letters S and L denote short and long sulfur bridge configuration, respectively.

explore the similarities and differences between two groups of isomers: short sulfur bridge conformers (S-form) and long sulfur bridge conformers (L-form). We calculated the electronic band structures of twenty-eight conformers, and predicted their detailed electronic properties. According to these calculations, we predict three structures of possible metallic conductors. Our subsequent DFT calculations also predict the probable structures of stable semiconducting configurations that have band gaps of less than 0.5 eV, and comparably unstable semi-metallic structures that have band gaps of less than 0.2 eV. To investigate atomic contributions to the electronic band structures, we performed the atom-pair analysis using the crystal orbital Hamilton population (COHP)[18,19] method to interpret which kinds of atom-pair interactions are critical to producing the electronic band structures and intramolecular charge migration. Once the exact atomic structures of $Mo_6S_3I_6$ are identified, we expect that $Mo_6S_3I_6$ nanowires will be used as unique nanoscale building blocks for a wide range of potential applications. As 2D TMDCs, they are likely to be useful for fabricating efficient nanoelectronics such as sensors, optoelectronic, transistors, and photovoltaic devices[20–24].

Results

Structural properties of new atomic models of $Mo_6S_3I_6$ nanowires. The initial structure of $Mo_6S_3I_6$ was prepared based on the previous research[10,12,14,17]. Structural parameters such as Mo-Mo bond lengths (3.24 Å) within the Mo_6 octahedron were taken from Karthikeyan *et al.*[14] Karthikeyan and coworkers also suggested that the bond length of Mo-S in the bridge positions (2.19 Å) is relatively shorter than those in the Mo_6 octahedron block. Using these parameters, we constructed an initial structure and then initially optimized it with a C_{3v} symmetry constraint by performing DFT calculations using PBE0 hybrid functional with def2-SV(P) basis set as implemented in Turbomole 7.2 program[25]. With this optimized structure, the further geometry optimizations are performed for the total 28 newly proposed atomic configurations in a hexagonal unit cell, in which the initial lattice constants are a = b = 15 Å, c = 12.5 Å and 13.75 Å. All the optimized lattice constants are determined by the volume and the ion relaxation processes for the total atomic models and reported as Table S1 in the supplementary information (SI). The two Mo_6 octahedra in the unit cell have the same structure in C_{3v} symmetry but are rotated by 180° from each other.

The initial structure of $Mo_6S_3I_6$ nanowire for structural calculations is shown in Fig. 1(a): it is composed of the two Mo_6 octahedra decorated by S- and I- atoms at the positions labeled by A*i*, A′*i*, B*j*, and B′*j*, $i = 0–3$, $j = 1–6$; ($i = 0$ refers to no sulfur atoms but three iodine atoms in the bridging plane). To begin with, the sulfur atoms in

#Of Sulfurs in Bridging Plane	0			1								2		3
Models	S (L) 0–1	S (L) 0–2	S (L) 0–3	S (L) 1–1	S (L) 1–2	S (L) 1–3	S (L) 1–4	S (L) 1–5	S (L) 1–6	S (L) 1–7	S (L) 1–8	S (L) 2–1	S (L) 2–2	S (L) 3–1
A1	I	I	I	S	S	I	I	I	I	I	S	I	S	S
A2	I	I	I	I	I	S	S	S	I	I	I	S	S	S
A3	I	I	I	I	I	I	I	I	I	S	I	S	I	S
A′1	I	I	I	I	I	I	I	I	I	S	I	S	I	S
A′2	I	I	I	I	I	I	S	S	I	I	I	S	S	S
A′3	I	I	I	S	S	S	I	I	I	I	S	I	S	S
B1	I	I	I	I	I	S	S	I	I	I	I	I	I	I
B2	I	S	S	S	I	I	I	S	I	I	I	I	I	I
B3	I	I	I	I	S	I	I	I	I	I	I	I	I	I
B4	S	S	I	I	I	I	I	I	I	I	I	S	S	I
B5	S	I	S	I	I	I	I	I	I	S	S	I	I	I
B6	S	S	S	S	S	S	S	S	I	S	S	I	I	I
B′1	I	S	I	I	I	S	S	S	I	I	I	I	I	I
B′2	I	I	I	I	S	I	I	I	I	I	I	I	I	I
B′3	I	S	S	S	I	I	I	I	I	I	I	I	I	I
B′4	S	I	I	I	I	I	I	I	I	S	S	I	I	I
B′5	S	I	S	S	S	I	S	S	I	S	S	I	I	I
B′6	S	S	S	S	I	S	I	I	I	I	I	S	S	I

Table 1. Atomic arrangement for various models of either short (S) or long (L) sulfur bridge configurations of $Mo_6S_3I_6$ nanowires. A*i*, A′*i*, B*j*, B′*j* represent the sites of sulfur or iodine atoms decorating the Mo_6 octahedron. The sulfur atoms in the bridging plane are assigned at A*i* and A′*i* and then the remaining S and I atoms are distributed in different permutations.

the bridging plane linked to the two Mo_6 octahedra are placed at both P3 and P6 layers, varying *i* from 0 to 3. In this step, the maximum number of sulfur atoms can be no more than three in P3 or P6 layer but the positions of sulfur atoms can be different from P3 and P6 layers. The rest of sulfur atoms and the remaining twelve iodine atoms are assigned to the sites determined by the periodicity of nanowires and molecular symmetry kept in their stoichiometry of $Mo_6S_3I_6$ composition. Consequently, the total of twenty-eight possible atomic models are studied in this work.

$Mo_6S_3I_6$ nanowires have large inter-chain separations with van der Waals (weak) interactions between the chains, and the nanowires are elastic in the direction along the chains[10]. We calculated the total energy of our targeted nanowire as a function of the lattice constant c and the results are presented in Fig. 1(b). The initial structure is uniformly elongated along the uniaxial axis and the two structural energy minima were found at lattice constants c = 12.50 Å, and 13.75 Å due to bi-stability of the S_3 linkages[17]. Though the two structural minima are very close in energy with the energy difference of only 0.03 eV/unit cell, the conformer with lattice constant c = 12.5 Å, is more stable and denoted as S (short form) and the other conformer is denoted L (long form). Accordingly, we hypothesized that the atomic configuration with which the S- and I- atom have in a unit cell would be important in determining not only the total energy but also the electronic structure of the nanowires.

Table 1 presents a summary of the possible atomic model configurations labeled by the following convention: The first letter 'S' or 'L' represent short and long sulfur bridge conformers, respectively, of the $Mo_6S_3I_6$ nanowires, and is followed by the number of sulfur atoms in the bridging plane. The additional number following the hyphen labels each of the possible conformers for that number of sulfur atoms in the bridging plane; zero, one, two, and three sulfur atoms in the bridging plane correspond to a total of three, eight, two, and one possible conformers, respectively. Finally, the optimized structure of these 28 atomic models are determined (Fig. 2).

The energies of S-form and L-form conformers are presented within a precision of 10^{-2} eV/unit cell for a given atomic composition. The short form conformers with only one sulfur atom in the S_3 bridging plane (S1-*k*, *k* = 1–8) are more stable (by about 5 eV/unit cell) than the short form conformer with three sulfur atoms in the bridging plane (S3–1). We found that the S3–1 conformer, which we used as the initial structure, is the highest in energy of all the proposed structures and is therefore the least stable. It is noteworthy that the energies of S0-*k* series are lower than those of the S3–1 conformers, so the conformers with I_3 linkages are more stable than the ones with S_3 linkages, which is different from the previous research[17].

The characteristic feature of the optimized structures for eight conformers of the calculated S1-*k* (*k* = 1–8) series is that the conformers are distorted during the ionic relaxation due to the displacement of the sulfur atom in the bridging plane towards the center of the bridge. This happens because the bridge tries to make the possible connection through the Mo-S bond, which is extended from 2.32 Å to 2.54 Å. In addition, the angle of Mo-S-Mo at the trigonal planar in the S_3 linkage plane that is perpendicular to the z-axis is found to change from 60 to 119.71 degrees. The unstable nanowire structures turned out to be better conductors through the ionic relaxation. Similarly, L-form structures with corresponding configurations have the same tendencies as the S-form structures regarding the displacement of their structures on a small scale. However, there is quite a remarkable distortion in the L1–7 conformer to make a strong overlap between Mo-S atoms. Like L1–7 conformers, a few of S-form

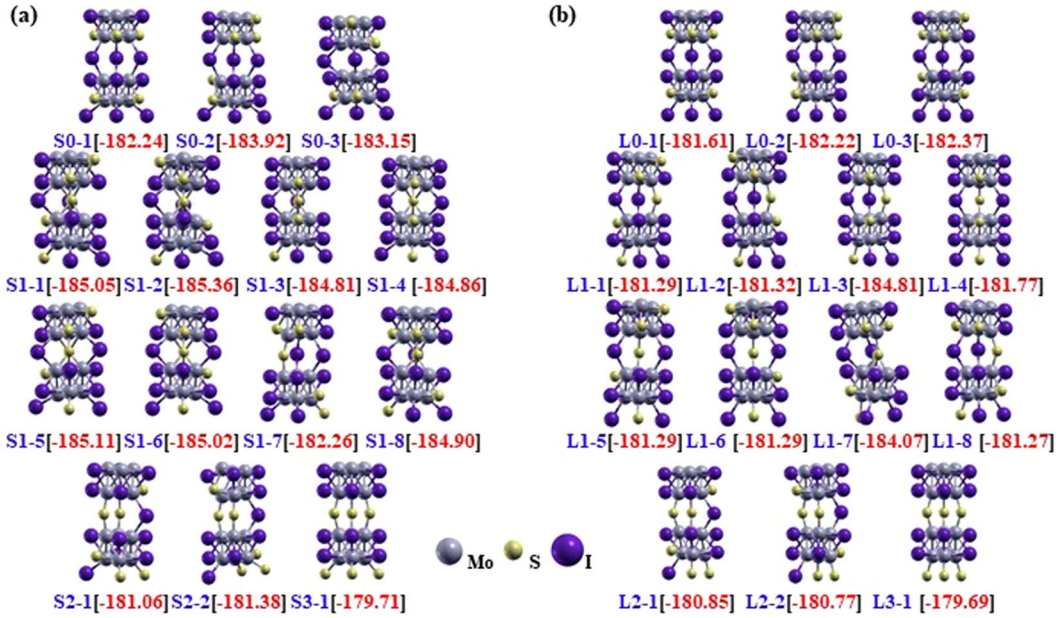

Figure 2. Ball and stick models of the optimized structures of various atomic $Mo_6S_3I_6$ nanowires identified in Table 1 with their total energies (eV/unit cell) indicated in square brackets for (**a**) S-form conformers (c = 12.5 Å), and (**b**) L-form conformers (c = 13.75 Å) of $Mo_6S_3I_6$ nanowires.

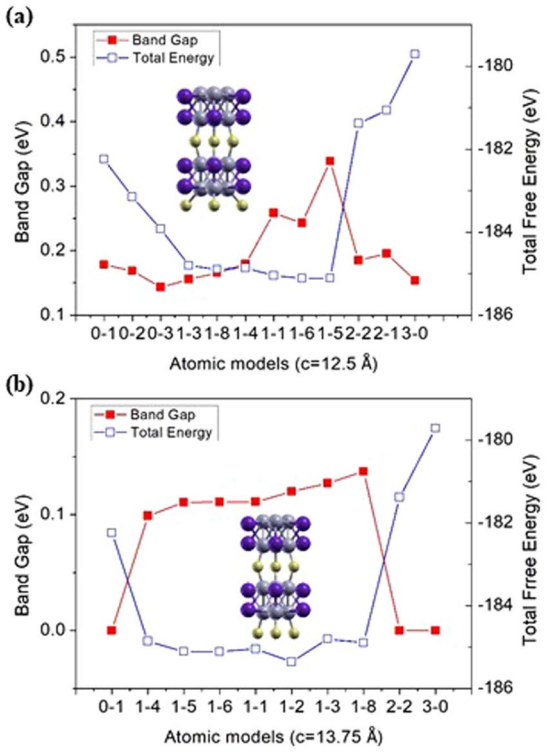

Figure 3. Electronic band gap energy and total energy per unit cell of various atomic models for (**a**) S-form conformers (c = 12.5 Å), and (**b**) L-form conformers (c = 13.75 Å) of $Mo_6S_3I_6$ nanowires. The red line denotes the band gap energy, and the blue line denotes the total energy of $Mo_6S_3I_6$ nanowire.

and L-form conformers are hard to be bound due to their deviation in the linear correlation so that they were excluded in Fig. 3.

The total energies per unit cell of various atomic models of $Mo_6S_3I_6$ nanowires are plotted as a function of their calculated electronic band gap energies E (k) in Fig. 3. It can be seen that the total energy is inversely related to the electronic band gap energy. This implies that the structural stability and the electronic band gap of the nanowires

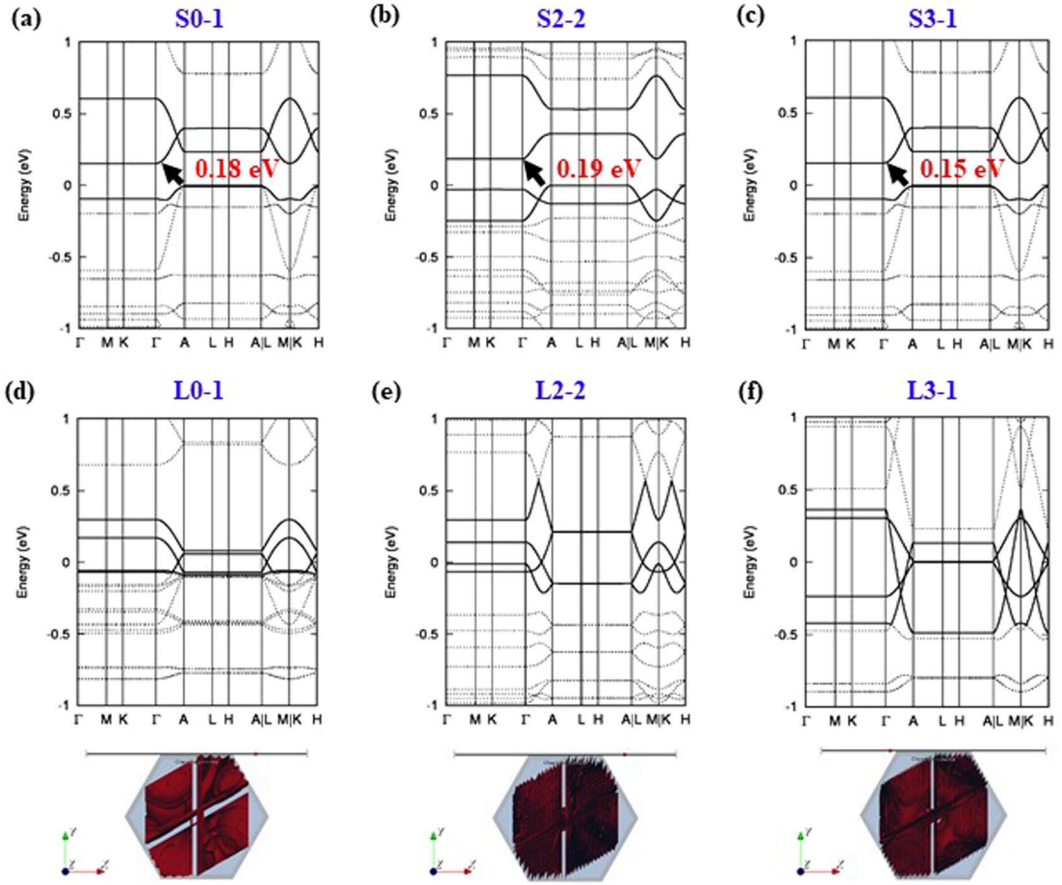

Figure 4. Electronic band structure of (**a**) S0–1, (**b**) S2–2, (**c**) S3–1, (**d**) L0–1, (**e**) L2–2, and (**f**) L3–1 conformers of a $Mo_6S_3I_6$ nanowire. The conduction and valence bands are emphasized by bold lines. While (**a**–**c**) are semiconductors, (**d**–**f**) are all metallic conductors, whose Fermi surfaces at each Fermi energy are shown below their electronic band structures with 3 times denser k-meshes using the interpolation method implemented in BolzTrap2[46] program. The Fermi surface for L0–1 is less dense than the ones for L2–2 and L3–1 conformers. The characteristic feature is to have a bridging connection in the middle of Fermi surfaces for those three metallic conformers shown in (**d**–**f**).

are inversely correlated. This relationship is due to not only van der Waals interactions between the bridge chains but also polar covalent bonds through the hybridization between the valence orbitals[14].

Electronic properties of new atomic models of $Mo_6S_3I_6$ nanowire. Electron transport through the bridge chains in a $Mo_6S_3I_6$ nanowire is known to be important for potential applications in molecular electronics[10–14,17]. To understand the effect of compositional variation on electron transport, the electronic structures and corresponding properties of the newly proposed atomic models of $Mo_6S_3I_6$ nanowire were investigated.

The electronic band structure along with reciprocal symmetry lines of S-form conformers and those of the corresponding L-form conformers are shown in Fig. 4. It is apparent that S0–1, S2–2, S3–1 conformers are narrow-gap semiconductors having band gap energies of 0.18 eV, 0.19 eV, and 0.15 eV, respectively. Of the conformers studied, the band gap of the S1–5 conformer is the largest at 0.34 eV, while that of the S3–1 conformer is the smallest of the S-form conformers (see Figs S8 and S14 in SI). The band gap energy is larger for more stable structures. It is more obvious that structural stability is inversely correlated with the electronic band gap in the case of L-form conformers, as presented in Fig. 3. Since the most of band gap energies in L-form conformers are all less than 0.2 eV, the L-form conformers can be regarded as narrow-gap semiconductors. The band structures of other atomic models in S-form and L-form conformers are presented in SI (see Figs S1–S28 in SI).

Figure 5(a–c) display the projected density of states (pDOS) of a $Mo_6S_3I_6$ nanowire in the energy range of $-0.1\,eV \leq E\text{-}E_F \leq 0.1\,eV$. The Fermi energy ($E_F$) is close to the top of the valence band and crosses the hybridized bands belonging to molybdenum, sulfur, and iodine. Small dispersion of the sub-bands together with the finite DOS at E_F is responsible for the semi-metallic and metallic transport properties of these nanowires[14]. Since the DOS at E_F is nonzero, we could expect that L0–1, L2–2, and L3–1 conformers are conductors that could be varied by their composition and elongation of the nanowire. It is supposed that a periodic distortion of the bond lengths somehow influences the behavior of the electrons in these systems because of a Peierls instability[26,27]. We find that structural instability causes the fluctuations of charge density waves[28,29]. As the electron density at E_F increases,

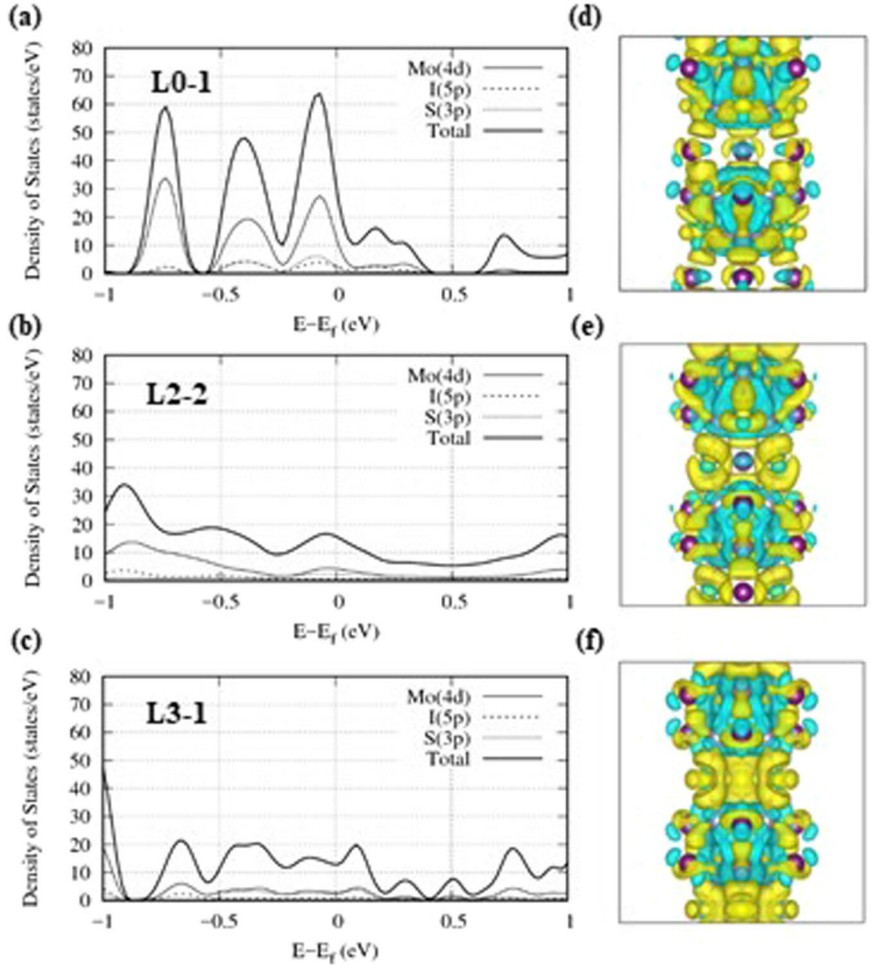

Figure 5. Projected density of states (pDOS) for three metallic conformers, (**a**) L0–1, (**b**) L2–2, and (**c**) L3–1 of a $Mo_6S_3I_6$ nanowire. The contributions of Mo, S, and I atoms are plotted individually for comparison. The main contributions to the conduction band are from Mo-4d, S-3p, and I-5p orbitals. (**d**–**f**) Valence charge density differences (VCDDs) in the three corresponding metallic conformers at c = 13.75 Å of $Mo_6S_3I_6$ nanowire. The yellow and cyan denote regions of charge depletion and excess, respectively, with respect to the superposition of isolated atoms.

the number of band crossings at the Fermi level increases. Several interpenetrating sub-bands, three in particular, cross the Fermi level through the reciprocal symmetry line of Γ-A as shown in Fig. 4(d–f).

Close to the Fermi level, the hybridization of Mo-4d, S-3p, and I-5p contributes to forming quasi-1D sheets[27,28] or Fermi surfaces. It is obvious that the electron density close to the Fermi level of the L3–1 conformer is the highest, and is more equally distributed than the L0–1 conformer as shown in Fig. 5(a–c). It causes that the Fermi surface for L0–1 is less dense than the ones for L2–2 and L3–1. It is noteworthy that the DOS at E_F is important for Fermi surfaces because there are sub-bands penetrating through the Fermi level. The pDOS of the calculated atomic models are presented in SI (see Figs S1–S28 in SI).

So far, the effect of the compositional variation on electron transport, electronic structures of our newly proposed $Mo_6S_3I_6$ nanowire configurations have been discussed. Moreover, the impact of the Mo-S bridge chains in a $Mo_6S_3I_6$ nanowire on charge density must also be understood for future applications.

The valence charge density differences (VCDDs) are calculated as a difference between the total charge density of the system and the superposition of the valence charge densities of neutral atoms[30]. The valence charge density differences in three metallic conformers are shown in Fig. 5(d–f). The yellow presents an accumulation of negative charges, whereas cyan denotes a depletion of charges as compared to neutral atoms. It is clearly seen that the excess valence charges between Mo-S bridge chains increase from the L0–1 to the L3–1 conformers. As the excess charge densities between molybdenum and sulfur atoms in the bridging plane increase, the nanowires are expected to become better conductors due to their electron delocalization. Since the conduction band charge of the Mo-4d orbitals is mostly rich enough to be transferred to the sulfur atoms through the polar covalent bond of Mo-S[11], we guess that the Mo-S interaction plays a key role in charge transport.

Previous studies with partial DOS have elucidated the electronic structures of these materials, however, the nature of states at the Fermi level have not been characterized by chemical-bonding analysis[31,32]. Using crystal orbital Hamilton population (COHP) curves implemented in the Local-Orbital Basis Suite Towards

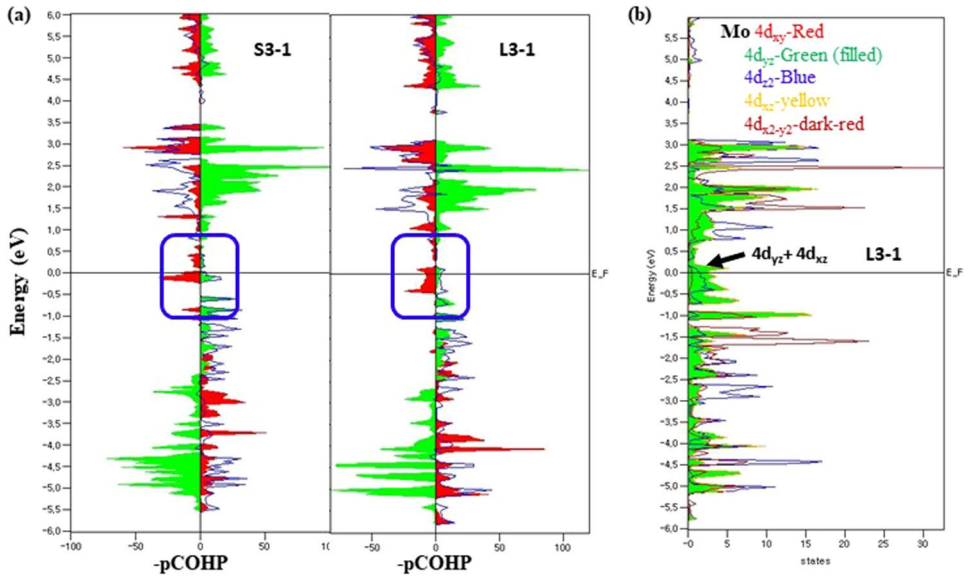

Figure 6. (**a**) The atom-projected crystal orbital Hamilton population (pCOHP) of S3–1 vs L3–1 conformers of a $Mo_6S_3I_6$ nanowire. The bonding orbital-pair interactions are presented on the right side of the panel, while the antibonding interactions are on the left side. The pCOHP of Mo-4d and S-3p are indicated as blue lines and red filled shadows, respectively, whereas the contributions from I-5p states are indicated as filled green shadows with sign flips for better comparison. (**b**) The orbital-pDOS of Mo-4d for the L3-1 metallic conformer. The red, filled green, blue, yellow, and dark-red denote $4d_{xy}$, $4d_{yz}$, $4d_{z2}$, $4d_{xz}$, and 4_{dx2-y2} orbital contributions, respectively. The energy axis is shown relative to the Fermi level.

Electronic-Structure Reconstruction (LOBSTER) package[31,33], we obtained the information about bonding and antibonding contributions of our targeted $Mo_6S_3I_6$ nanowires by re-extracting the atom-resolved information from delocalized plane-wave basis sets.

The atom-pCOHP of the S3–1 and L3–1 conformers of a $Mo_6S_3I_6$ nanowire are shown in Fig. 6(a). The diagram of COHP reveals a stabilizing or destabilizing energy criterion that converts the DOS into both negative for bonding and positive for antibonding values, in contrast to the conventional DOS, which yields the number of electrons in the system[32]. As shown in Fig. 6(a), the orbital energy is plotted as a function of the negative value of projected crystal orbital Hamilton population (–pCOHP) for convenience. Molybdenum shows the bonding character, but the sulfur and iodine show the antibonding character both in the valence band and near the Fermi level. Particularly, a much larger antibonding character of the sulfur atoms can be found near the Fermi level compared to that of iodine atoms; the antibonding character of sulfur atoms contributes to the metallic nature of a $Mo_6S_3I_6$ nanowire by destabilizing the band structure energy. In addition, it is obvious that the dominant contributions are from $4d_{yz}$ and $4d_{xz}$ orbitals of Mo as shown in Fig. 6(b). We found that the sulfur contributions are mainly from $3p_x$ and $3p_y$ orbitals, and from $5p_x$ and $5p_y$ orbitals for iodine (see Fig. S29 in SI).

COHP partitions the band-structure energy into orbital-pair interactions between a pair of adjacent atoms. A COHP diagram indicates bonding and antibonding contributions to the band-structure energy in terms of DOS that usually shows where electrons are in a system. Whereas COHP shows the contribution of a specific bond to the band energy, the integrated COHP (ICOHP) gives a hint towards the bond strength in energy unit (eV).

Figure 7 shows the relationship between ICOHP and band gap energy for the L3–0 conformer of a $Mo_6S_3I_6$ nanowire based on the type of atom-pair interactions. For the Mo-S atom-pair bonding interaction, it is apparent that an increase in the bonding orbital energy stabilizes the band structure energy, which leads to an increase of the band gap energy. On the other hand, this is not the case for the Mo-I atom-pair interaction. Our work shows that the Mo-S bonding interaction is mainly responsible for not only the structural stability but also the electronic properties of $Mo_6S_3I_6$ nanowire. The pCOHP of atom-pair interaction (Mo-Mo, Mo-S, and Mo-I) of newly proposed atomic models are presented in SI. (see Figs S30–S57 in SI).

Conclusion

We investigated the effect of structural disorder on $Mo_6S_3I_6$ nanowires by compositional modeling for two local energy minima structures identified by the elongation of the bridge chains. Based on the two stable structures, we performed DFT calculations to explore the impact of sulfur or iodine atom locations on the electronic properties of the newly proposed atomic models. In this paper, we report the structural properties, electronic band structures, and pDOS of our newly proposed atomic models. We showed that the electronic band gap energy is inversely correlated to structural stability, and introduced Fermi surfaces for the three structures with a lattice constant of c = 13.75 Å that are possible conductors. As the delocalized valence charge density differences are increased through the Mo-S bridging chains, the electron densities at the Fermi level are also increased. This implies that the existence of sulfur atoms in the bridging plane plays an important role in the intramolecular

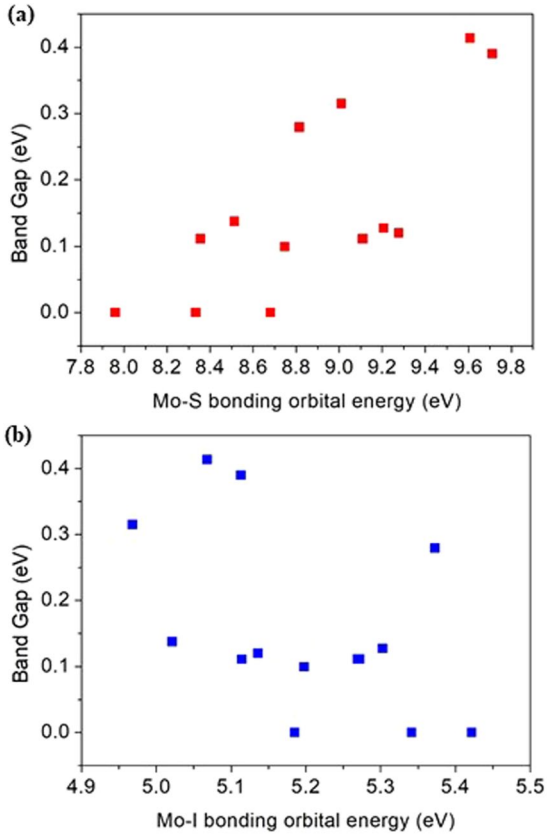

Figure 7. The relationship between integrated crystal orbital Hamilton populations (ICOHP) and the band gap energy of the L3–1 conformer for (**a**) Mo-S interactions, and (**b**) Mo-I interactions.

charge transport. Our theoretical calculations using crystal orbital Hamilton populations (COHP) analysis predict that the electronic band gap energy of a $Mo_6S_3I_6$ nanowire is quite linearly correlated with Mo-S bonding or antibonding orbital energy due to the structural stability. Since compositional variation can be used to control the Mo-S bonding interactions, isolated or bundled $Mo_6S_3I_6$ nanowires are expected to be utilized as essential components of a wide range of applications such as optoelectronics, transistors, sensors, and photovoltaic devices[20–24,34] in near-term.

Methods

To investigate the structural and electronic properties of an isolated $Mo_6S_3I_6$ nanowire, we performed DFT calculations with projected augmented wave method[35,36] and a plane-wave basis set as implemented in the Vienna *Ab initio* Simulation Package (VASP)[37–40]. The electron-electron correlation energy was corrected by the Perdew, Burke, and Enzerhoff (PBE) generalized gradient approximation (GGA)[41,42]. Ionic and electronic relaxations were carried out using an iterative conjugate gradient minimization method. The energy cut-off was chosen to be 500 eV, and Gaussian smearing for geometry optimization and Fermi smearing for band structure calculations with Blöchl correction were used with a 0.05 eV smearing width. To describe the infinite isolated nanowires with a different compositional arrangement, we placed nanowires in a large hexagonal unit cell with 15 Å vacuum space in the *x*- and *y*-directions to limit inter-wire interactions. All geometries were optimized without any symmetry constraints. The Brillouin zone was sampled by $1 \times 1 \times 14$ Γ-centered automatic *k*-meshes to converge the ionic relaxation calculation and 100 *k*-points along the reciprocal symmetry lines to obtain the DOS. The Mo-4d, S-3p, and I-5p electrons are considered to be valence electrons not only for the pDOS but also for the calculation of crystal orbital Hamilton population, which is employed for the analysis of bonding and antibonding orbital energy and the interaction between specific atoms. In addition to VASP, Xcrysden[43,44], wxDragon[45] and LOBSTER[31,32] were employed for visualizing the calculation results.

References

1. Potel, M. *et al.* New pseudo-one-dimensional metals: $M_2Mo_6Se_6$ (M = Na, In, K, TI), $M_2Mo_6S_6$ (M = K, Rb, Cs), $M_2Mo_6Te_6$ (M = In, TI). *J. Solid. State. Chem.* **35**, 286–290 (1980).
2. Brusetti, R., Monceau, P., Potel, M., Gougeon, P. & Sergent, M. The exotic superconductor $Tl_2Mo_6Se_6$ investigated by low field magnetization measurements. *Solid. State. Commun.* **66**, 181–187 (1988).
3. Venkataraman, L. & Lieber, C. M. Molybdenum Selenide Molecular Wires as One-Dimensional Conductors. *Phys. Rev. Lett.* **83**, 5334–5337 (1999).
4. Remskar, M. *et al.* Self-Assembly of Subnanometer-Diameter Single-Wall MoS_2 Nanotubes. *Science* **292**, 479 (2001).

5. Ribeiro, F. J., Roundy, D. J. & Cohen, M. L. Electronic properties and ideal tensile strength of MoSe nanowires. *Phys. Rev. B* **65**, 153401 (2002).
6. Kis, A. *et al*. Shear and Young's Moduli of MoS_2 Nanotube Ropes. *Adv. Mater.* **15**, 733–736 (2003).
7. Wang, H. *et al*. Two-dimensional heterostructures: fabrication, characterization, and application. *Nanoscale* **6**, 12250–12272 (2014).
8. Schwierz, F., Pezoldt, J. & Granzner, R. Two-dimensional materials and their prospects in transistor electronics. *Nanoscale* **7**, 8261–8283 (2015).
9. Daniel, V. *et al*. Air-stable monodispersed $Mo_6S_3I_6$ nanowires. *Nanotechnology* **15**, 635 (2004).
10. Vilfan, I. & Mihailovic, D. Nonlinear elastic and electronic properties of $Mo_6S_3I_6$ nanowires. *Phys. Rev. B* **74**, 235411 (2006).
11. Yang, T., Okano, S., Berber, S. & Tománek, D. Interplay between Structure and Magnetism in $Mo_{12}S_9I_9$ Nanowires. *Phys. Rev. Lett.* **96**, 125502 (2006).
12. Yang, T., Berber, S. & Tománek, D. Compositional ordering and quantum transport in $Mo_6S_{9-x}I_x$ nanowires: *Ab initio* calculations. *Phys. Rev. B* **77**, 165426 (2008).
13. Kang, S.-H., Kwon, Y.-K. & Tomanek, D. Effect of bundling on the stability, equilibrium geometry, and electronic structure of $Mo_6S_{9-x}I_x$ nanowires. *Phys. Rev. B* **82** (2010).
14. Karthikeyan, J., Kumar, V. & Murugan, P. The Role of Valence Electron Concentration in Tuning the Structure, Stability, and Electronic Properties of $Mo_6S_{9-x}I_x$ Nanowires. *J. Phys. Chem. C* **119**, 13979–13985 (2015).
15. Marko, Ž. *et al*. Field emission of point-electron source $Mo_6S_3I_6$ nanowires. *Nanotechnology* **16**, 1619 (2005).
16. Paglia, G., Božin, E. S., Vengust, D., Mihailovic, D. & Billinge, S. J. L. Accurate Structure Determination of $Mo_6S_yI_z$ Nanowires from Atomic Pair Distribution Function (PDF) Analysis. *Chem. Mater.* **18**, 100–106 (2006).
17. Kang, S.-H., Kwon, Y.-K. & Tománek, D. Interplay between structural and electronic properties of bundled $Mo_6S_{9-x}I_x$ nanowires. *J. Phys.: Conden. Matt.* **22**, 505301 (2010).
18. Dronskowski, R. & Bloechl, P. E. Crystal orbital Hamilton populations (COHP): energy-resolved visualization of chemical bonding in solids based on density-functional calculations. *J. Phys. Chem.* **97**, 8617–8624 (1993).
19. Deringer, V. L., Tchougréeff, A. L. & Dronskowski, R. Crystal Orbital Hamilton Population (COHP) Analysis As Projected from Plane-Wave Basis Sets. *J. Phys. Chem. A* **115**, 5461–5466 (2011).
20. Splendiani, A. *et al*. Emerging Photoluminescence in Monolayer MoS_2. *Nano Lett.* **10**, 1271–1275 (2010).
21. McMullan, M. *et al*. Aptamer conjugated $Mo_6S_{9-x}I_x$ nanowires for direct and highly sensitive electrochemical sensing of thrombin. *Biosens. and Bioelectron.* **26**, 1853–1859 (2011).
22. Majkić, A. *et al*. $Mo_6S_{9-x}I_x$ nanowires as additives for enhanced organic solar cell performance. *Sol. Energy Mater. and Sol. Cells* **127**, 63–66 (2014).
23. Tsai, M.-L. *et al*. Monolayer MoS_2 Heterojunction Solar Cells. *ACS Nano* **8**, 8317–8322 (2014).
24. Buscema, M. *et al*. Photocurrent generation with two-dimensional van der Waals semiconductors. *Chem. Soc. Rev.* **44**, 3691–3718 (2015).
25. Ahlrichs, R., Bär, M., Häser, M., Horn, H. & Kölmel, C. Electronic structure calculations on workstation computers: The program system turbomole. *Chemical Physics Letters* **162**, 165–169 (1989).
26. Toombs, G. A. Quasi-one-dimensional conductors. *Phys. Rep.* **40**, 181–240 (1978).
27. Prodan, A. *et al*. Charge density waves in $NbSe_3$: The models and the experimental evidence. *Solid. State. Commun.* **150**, 2134–2137 (2010).
28. Jiang, H., Cao, G. & Cao, C. Electronic structure of quasi-one-dimensional superconductor $K_2Cr_3As_3$ from first-principles calculations. *Sci. Rep.* **5**, 16054 (2015).
29. Bao, J.-K. *et al*. Superconductivity in Quasi-One-Dimensional $K_2Cr_3As_3$ with Significant Electron Correlations. *Phys. Rev. X* **5**, 011013 (2015).
30. Wu, H.-Y. *et al*. Interfacial Interaction between Boron Cluster and Metal Oxide Surface and Its Effects: A Case Study of B_{20}/Ag_3PO_4 van der Waals Heterostructure. *J. Phys. Chem. C* **122**, 6151–6158 (2018).
31. Maintz, S., Deringer, V. L., Tchougréeff, A. L. & Dronskowski, R. Analytic projection from plane-wave and PAW wavefunctions and application to chemical-bonding analysis in solids. *J. Comput. Chem.* **34**, 2557–2567 (2013).
32. Nelson, R., Konze, P. M. & Dronskowski, R. First-Principles Chemical Bonding Study of Manganese Carbodiimide, MnNCN, As Compared to Manganese Oxide, MnO. *J. Phys. Chem. A* **121**, 7778–7786 (2017).
33. Maintz, S., Deringer, V. L., Tchougréeff, A. L. & Dronskowski, R. LOBSTER: A tool to extract chemical bonding from plane-wave based DFT. *J. Comput. Chem.* **37**, 1030–1035 (2016).
34. Radisavljevic, B., Radenovic, A., Brivio, J., Giacometti, V. & Kis, A. Single-layer MoS_2 transistors. *Nat. Nanotechnol.* **6**, 147 (2011).
35. Blöchl, P. E. Projector augmented-wave method. *Phys. Rev. B* **50**, 17953–17979 (1994).
36. Kresse, G. & Joubert, D. From ultrasoft pseudopotentials to the projector augmented-wave method. *Phys. Rev. B* **59**, 1758–1775 (1999).
37. Kresse, G. & Hafner, J. *Ab initio* molecular dynamics for liquid metals. *Phys. Rev. B* **47**, 558–561 (1993).
38. Kresse, G. & Hafner, J. *Ab initio* molecular-dynamics simulation of the liquid-metal–amorphous-semiconductor transition in germanium. *Phys. Rev. B* **49**, 14251–14269 (1994).
39. Kresse, G. & Furthmüller, J. Efficiency of ab-initio total energy calculations for metals and semiconductors using a plane-wave basis set. *Comput. Mater. Sci.* **6**, 15–50 (1996).
40. Kresse, G. & Furthmüller, J. Efficient iterative schemes for *ab initio* total-energy calculations using a plane-wave basis set. *Phys. Rev. B* **54**, 11169–11186 (1996).
41. Perdew, J. P., Burke, K. & Ernzerhof, M. Generalized Gradient Approximation Made Simple. *Phys. Rev. Lett.* **77**, 3865–3868 (1996).
42. Perdew, J. P., Burke, K. & Wang, Y. Generalized gradient approximation for the exchange-correlation hole of a many-electron system. *Phys. Rev. B* **54**, 16533–16539 (1996).
43. Kokalj, A. XCrySDen—a new program for displaying crystalline structures and electron densities. *J. Mol. Graph. and Model.* **17**, 176–179 (1999).
44. Kokalj, A. Computer graphics and graphical user interfaces as tools in simulations of matter at the atomic scale. *Comput. Mater. Sci.* **28**, 155–168 (2003).
45. Gonze, X. *et al*. ABINIT: First-principles approach to material and nanosystem properties. *Comput. Phys. Commun.* **180**, 2582–2615 (2009).
46. Madsen, G. K. H., Carrete, J. & Verstraete, M. J. BoltzTraP2, a program for interpolating band structures and calculating semi-classical transport coefficients. *Comput. Phys. Commun.* **231**, 140–145 (2018).

Acknowledgements

This work was supported by the National Research Foundation of Korea (NRF) grant funded by the Korea government (MSIP) (No. NRF-2017R1A4A1015770).

Author Contributions

Y.K.C., W.-G.L. and S.C. conducted experiments, analyzed the data and wrote the paper. J.-Y.C. and J.H. conceived and designed the experiments, worked on the theory, analyzed the data and wrote the paper.

Additional Information

Supplementary information accompanies this paper at https://doi.org/10.1038/s41598-018-37818-7.

Competing Interests: The authors declare no competing interests.

Publisher's note: Springer Nature remains neutral with regard to jurisdictional claims in published maps and institutional affiliations.